J Solid State Electrochem (2006) 10: 547–561
DOI 10.1007/s10008-006-0135-x

ORIGINAL PAPER

Bjarke Dalslet · Peter Blennow · Peter Vang Hendriksen · Nikolaos Bonanos · Dorthe Lybye · Mogens Mogensen

Assessment of doped ceria as electrolyte

Received: 17 January 2006 / Accepted: 31 January 2006 / Published online: 13 May 2006

Abstract A model describing the performance of a fuel cell based on 10 mol% gadolinia-doped ceria, $Ce_{0.9}Gd_{0.1}O_{1.95-x}$ (CG10), was formulated. The total electrical conductivity of CG10 was measured under very reducing conditions in the temperature range of 753 K to 948 K. Oxygen permeation experiments were carried out to measure the leak current through a ceria electrolyte. The results of the measurements are compared with predictions of the formulated model. Furthermore, the response of a fuel cell to changing operating conditions such as external load, temperature, electrode polarization resistances, and defect chemistry is investigated using the model. It is found that the maximum achievable efficiency of a CG10-based fuel cell is increased when (1) the temperature is decreased, when (2) the electrolyte thickness is increased, or when (3) the cathode polarization resistance is decreased. The efficiency can also in certain circumstances be increased by an increase of anode polarization resistance. Finally, the efficiency is reduced if the vacancy formation enthalpy is decreased to the level of fine-grained CG10. The performance of a CG10-based cell is evaluated by comparing it with a state-of-the-art zirconia-based cell. At 873 K, the efficiency of a fuel cell with a 10-μm CG10 electrolyte was limited to 0.74, whereas a cell with a perfect electrolyte would have an efficiency of 1. The power output of the CG10 cell at this efficiency is, however, four times larger than the zirconia-based cell at the same efficiency. This is due to the much lower cathode polarization resistance of $(La_{0.6}Sr_{0.4})_zCo_{0.2}Fe_{0.8}O_{3-\delta}$ -CG10 cathodes on CG10 compared to the $(La_{0.75}Sr_{0.25})_{0.95}MnO_3$ cathodes on stabilized zirconia.

Keywords Electrolytes · Electrochemistry · Fuel cells

B. Dalslet (✉) · P. Blennow · P. V. Hendriksen · N. Bonanos · D. Lybye · M. Mogensen
Materials Research Department,
Frederiksborgvej 399,
P.O. Box 49, Roskilde 4000, Denmark
e-mail: Bjarke.dalslet@risoe.dk
Tel.: +45-46775883
Fax: +45-46775758

Introduction

Doped ceria, $Ce_{1-y}Re_yO_{2-y/2-x}$ (with Re=Gd, Sm, and $y<0.4$), is a well-known class of fast oxide ion conductors. Despite being an electronic conductor when exposed to reducing conditions at high temperatures [1], doped ceria has attracted renewed attention as an electrolyte in solid oxide fuel cells (SOFCs). Doped ceria has advantages over conventional zirconia oxide-based electrolytes in several areas such as higher ionic conduction at low temperature [2] and better chemical compatibility with high performance cathode materials such as $La_xSr_{1-x}Co_yFe_{1-y}O_{3-\delta}$ [3–5]. The degree to which doped ceria is a mixed ionic and electronic conductor (MIEC) varies with the doping level, temperature, and oxygen activity. High leak current densities may be deduced from reports on SOFCs with ceria-based electrolyte [6–8] in which open circuit voltage (OCV) values below 900 mV were observed at temperatures as low as 725 K using 97% H_2 + 3% H_2O fuel gas mixtures. Recently, however, ceria-based cells with high performance were demonstrated [9].

The ionic transport through an imperfect electrolyte such as $Ce_{0.9}Gd_{0.1}O_{1.95-x}$ (CG10) depends on several factors, many of which are interdependent. For instance, the vacancy concentration profile through the electrolyte affects the leak current, which affects the electrode polarizations, which closes the circle by affecting the vacancy concentration profile. These intimate relations complicate both the interpretation of measured data and identification of key areas in which to focus research [10]. Modeling of the ionic and electronic transport of the MIEC can provide better understanding of the phenomena involved in the transport. The literature contains several model studies of MIEC electrolytes and fuel cells [11–16].

This study considers a model of a cell with a CG10 electrolyte. To validate this model, measurements of the total conductivity of CG10 under very reducing conditions and the oxygen leakage through a CG10 disk are presented in this study. Further validation is performed by comparison of model results with measurement data reported in the

literature. Individual model parameters are varied one at a time from a common reference state and the impact on cell performance is evaluated. The parameters varied are the external load resistor, the temperature, the oxide vacancy formation enthalpy, the electrode polarization resistances, and the thickness of the electrolyte. Finally, a comparison with a state-of-the-art doped zirconia electrolyte-based cell is made. The treatment will include conditions where CG10 is an electrolyte and conditions where it has a significant electronic conductivity. Nevertheless, the CG10 layer between the electrodes will be referred to as the "electrolyte" for ease of reading, even when it shows mixed conduction.

Theory and model description

Defect chemistry of CG10

In CG10 oxide, vacancies are created by the partial substitution of Ce^{4+} with Gd^{3+}. Stated in the Kröger–Vink notation, the reaction is

$$Gd_2O_3 \xrightarrow{CeO_2} 2Gd'_{Ce} + V^{\bullet\bullet}_O + 3O^X_O \quad (1)$$

Oxide vacancy formation by substitution contributes only ionic charge carriers.

Oxide vacancies can also be created as oxide ions interact with the gas-phase oxygen at the surfaces.

$$O^X_O + 2Ce^X_{Ce} \rightleftarrows \frac{1}{2}O_2 + V^{\bullet\bullet}_O + 2Ce'_{Ce} \quad (2)$$

Reducing the oxide activity in the material will create both electronic charge carriers $\left(Ce'_{Ce}\right)$ and ionic charge carriers $\left(V^{\bullet\bullet}_O\right)$ according to Eq. 2.

The oxide vacancy concentration of an oxide material is related to the oxygen partial pressure of a gas with which the material is in equilibrium. In equilibrium, the chemical potentials of the oxide and the gas are equal:

$$\Delta H(x) - T\Delta S(x) = \mu^0_{O_2}(T) + RT\ln pO_2 \quad (3)$$

where x is the number of oxide ions per formula unit, which were removed from the lattice by reduction of the stoichiometric oxide (in the case of CG10). $\Delta H(x)$ and $\Delta S(x)$ are the x-dependent enthalpy and entropy associated with oxide vacancy formation. $\mu^0_{O_2}(T)$ is the standard chemical potential of oxygen. T is the temperature in Kelvin and R is the gas constant. Ignoring the temperature-dependence of the chemical potential of oxygen in a gas, the relation can be rewritten:

$$\ln pO_2 = \frac{\Delta H(x)}{RT} - \frac{\Delta S(x)}{R} \quad (4)$$

If $\Delta H(x)$ and $\Delta S(x)$ are known, then x and with it both the electronic and ionic charge carrier concentrations can be calculated with Eq. 4.

Ambipolar transport model

Overview

The model used in this paper is outlined in Fig. 1. At the cathode, oxygen molecules from the cathode gas will dissociate, absorb electrons, and diffuse into the electrolyte as ions. This process is represented with a cathode polarization resistance, $r_{cathode}$. The oxide ions are then transported through the electrolyte to the anode. At the anode the oxide ions will be converted to anode gas molecules, shedding electrons in the process. This process is represented with an anode polarization resistance r_{anode}. The electrons will be transferred back to the cathode through either the external resistance or as leak current in the electrolyte.

Transport in the electrolyte

The transport in the electrolyte will be treated using the model published by Näfe [13]. This is a one-dimensional model of a MIEC membrane placed in an oxygen potential gradient. It is necessary to treat CG10 as a MIEC as it can have a significant electronic leak current. The model of Näfe is, as the Wagner model [17], constructed from the following requirements: (1) local and global charge balance; (2) current balance of the ionic, electronic, and external (electronic) currents; and (3) the difference of the electrochemical potential of electrons must equal FU between the electrodes, U being the voltage difference and F Faraday's number. Contrary to the Wagner model, the electrolyte in the model of Näfe can be connected with a parallel external resistance r_{ext}. In the case of a homogenous current density through the electrolyte, r_{ext} can be expressed as $r_{ext} = \frac{L}{\sigma_{ext}A}$ where L is the electrolyte width, A is the electrolyte area and σ_{ext} is the conductance of a load resistor of the same geometry as the electrolyte. Using the

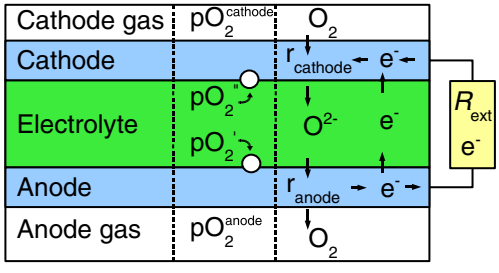

Fig. 1 The cell considered in the model. The *left column* shows the name of the cell parts. The *middle column* marks the pO_2 labels through the cell. The *right column* shows the current circuit of the cell

model of Näfe and rearranging the formulas, the internal electronic current density i_e can be calculated as:

$$i_e = -\frac{RT}{z_e z_i F N_O L}\int_{\ln pO_2'}^{\ln pO_2''} \frac{\sigma_e \sigma_i}{\sigma_i + (\sigma_e + \sigma_{ext})} d(\ln pO_2) \quad (5)$$

where z_i and z_e is the charge of the ionic species and electrons in units of e, F is Faraday's constant, N_O is the number of atoms per molecule in the gas phase (2 for oxygen), pO_2' and pO_2'' are the oxygen partial pressures of the electrolyte interfaces, (see Fig. 1), and σ_i and σ_e are the x-dependent conductivities of electrons and ions in the electrolyte. The internal electronic current density is often referred to as the leak current density.

The oxide ion current density can be written [13]:

$$i_i = -\frac{RT}{z_i N_O F L}\int_{\ln pO_2'}^{\ln pO_2''} \frac{\sigma_i(\sigma_e + \sigma_{ext})}{\sigma_i + (\sigma_e + \sigma_{ext})} d(\ln pO_2) \quad (6)$$

The quantity $\frac{\sigma_i(\sigma_e+\sigma_{ext})}{\sigma_i+(\sigma_e+\sigma_{ext})}$, which has the dimension of a conductivity but refers to the entire system including the load resistor, will be abbreviated Σ. As can be seen, the essence of the approach of Näfe is to treat the external electronic current density as if a second type of electron was running in the electrolyte. The gradient of the electrochemical potential of the electrons $\nabla\eta_e$ can be calculated as [13]:

$$\nabla\eta_e = -\frac{1}{z_i N_O}\frac{\sigma_i}{\sigma_i + (\sigma_e + \sigma_{ext})}\nabla\mu_{O_2} \quad (7)$$

In the case of electrodes with equal electron chemical potentials, the voltage U can be calculated by integration of Eq. 7. This integration reduces to the Nernst equation when $(\sigma_e + \sigma_{ext}) = 0$. This model of Näfe (Eqs. 5, 6, and 7) will be used in this study to calculate the ionic and electronic current densities in the electrolyte and the electric potential difference between the electrodes. The pO_2 boundaries of the integrations are dependent on the pO_2 of the surrounding gas and the polarization of the electrodes.

Electrode polarization resistance

The electrode kinetics will be modeled as two extra layers of matter with finite resistance on each side of the electrolyte. This electrode polarization resistance represents the summation of processes, which transforms an oxygen molecule from the surrounding gas to two oxide ions and four electrons in the MIEC. For simplicity, linear electrode kinetics and no resistance-dependence on the various concentrations in neither the gas phase nor electrode will be considered when modeling the electrodes. The ionic current density through the electrode layer can then be written:

$$i_i = \frac{1}{z_i F N_O}\frac{1}{r_{electrode}}\Delta(RT\ln pO_2) \quad (8)$$

where $r_{electrode}$ is the electrode polarization resistance. The cell is divided into discreet segments (100 bulk segments and 2 electrode segments) with each segment labeled with a pO_2. Equations 5, 6, 7, and 8 is solved under the requirement of a constant oxide, electron, and external electron current density for all the segments. The pO_2 on the fuel and airside provides the boundary conditions.

Power density and efficiency

To characterize the cell performance, two characteristic quantities are calculated:

- The power density of the fuel cell (p) is defined as the power dissipated in the external resistor. It is calculated as:

$$p = i_{ext} U \quad (9)$$

  where U is the voltage between the electrodes and i_{ext} is the current density in the external resistor.
- The efficiency η is defined as the product of the ratio of the cell voltage to the Nernst voltage $\frac{U}{U_{Nernst}}$ and the ratio of the external current density to the ionic current density $\frac{i_{ext}}{i_i}$:

$$\eta = \frac{U}{U_{Nernst}}\frac{i_{ext}}{i_i} \quad (10)$$

The efficiency is a normalized measure of the energy dissipated in the load resistor per oxygen molecule transferred from the cathode gas to the anode gas. An efficiency of 1 will correspond to a perfect electrolyte running at the Nernst voltage. In practical terms, the efficiency is a cell efficiency. It does not contain the inefficiency factors coming from fuel gas reformation, incomplete fuel exploitation, and auxiliary systems.

Using Kirchoff's law of current balance, U can be written in terms of U_{Nernst}, the current density, and the resistances:

$$U = U_{Nernst} - (r_{anode} + r_{cathode} + r_{ion})(i_{ext} + i_e) \quad (11)$$

where $r_{ion} = \int_{electrolyte}\frac{1}{\sigma_i}$. Combining Eqs. 10 and 11, the efficiency can be expressed as a function of resistances. The following substitutions are necessary: $r_e = U/i_e$, $i_i = i_{ext} + i_e$ and $r_{ext} = U/i_{ext}$.

$$\eta = \frac{1}{1 + (r_{\text{anode}} + r_{\text{cathode}} + r_{\text{ion}})\left(\frac{1}{r_{\text{ext}}} + \frac{1}{r_e}\right)} \cdot \frac{1}{1 + \frac{r_{\text{ext}}}{r_e}} \tag{12}$$

The first factor is the voltage efficiency and the second factor is the faradaic efficiency. One of the important parameters in the following analysis is the maximum possible efficiency $\eta_{\max}$. To find $\eta_{\max}$, r_{ext} is adjusted while the temperature, electrode polarization resistances, and gas mixtures are kept constant.

Reference cell

During this model study, a number of different cells will be investigated. In this section a reference cell is defined. If the cells deviate from the reference cell, it will be explicitly stated in the text.

Mogensen et al. [1] has evaluated values of $\Delta H(x)$ and $\Delta S(x)$ reported by several research groups. In this model study, the $\Delta H(x)$ and $\Delta S(x)$ reported by Wang et al. [18] are used.

Wang et al. [19] also reported values of the temperature-dependent mobilities of the ionic and electronic charge carriers in CG10. These values will be used in this model study and are given in Table 1. Wang et al. describes the large activation energy of $\mu_e T$ as abnormal, possibly due to defect association at high temperature. In this study, it will nevertheless be assumed that the activation energy is correct. For simplicity, the mobilities will be assumed to be independent of the concentration of vacancies. This is justified as the vacancy concentration will be almost constant if very reducing conditions ($pO_2 < 10^{-30}$ atm at 873 K) are avoided.

The polarization resistance measured on a composite yttrium-doped zirconia and nickel (Ni-YSZ) electrode in a hydrogen/water mixture will be used for the anode polarization resistance. The used value of the resistance was not published explicitly but can be rationalized from the work of Primdahl and Mogensen [20] and Barfod et al. [21]. Only the temperature-dependence is taken into account. Because Ni-CG10 electrodes would be expected to be the best choice for a CG10 electrolyte, it is assumed that it is possible to fabricate anodes of Ni-CG10, which is at least as good as the Ni-YSZ electrodes reported.

The cathode polarization resistance that was reported by Wang and Mogensen [3] for a $(La_{0.6}Sr_{0.4})_z Co_{0.2}Fe_{0.8}O_{3-\delta}$ CG10 (LSCF-CG10) composite cathode in air will be used.

Experimental

Total conductivity measurements

CGO10 powder from Rhodia was pressed isostatically into a pellet. The pellet was sintered at 1,773 K for 2 h standing on 8YSZ tape. The pellet was cut to a bar (2×3×5 mm) and ground to having parallel sides. Before measuring the conductivity, Pt-paste was applied as electrodes and the samples were heat-treated at 1,273 K for 1/2 h.

The conductivity was measured by pseudo four-point (using four wires connecting two electrodes) [22] impedance spectroscopy using a computer-controlled HIOKI 3522-50 LCR HiTESTER using the frequency range: 1 MHz–46 Hz. The impedance was measured at reducing conditions at temperatures between 753 K and 948 K and in air between 403 K and 1,273 K.

Oxygen permeation experiments

The oxygen permeation rates were measured on a sample of tapecast CGO10 of thickness 210 μm, produced by ECN Netherlands, equipped with an anode of NiO/CGO10 and a cathode of $(La_{0.6}Sr_{0.4})_{0.9}Co_{0.2}Fe_{0.8}O_3/Ce_{0.9}Gd_{0.1}O_2$ (LSCF/CGO10). The sample was sealed on to an Al_2O_3 tube using a ring of tapecast, powdered glass with a softening point of ca 880 K. The arrangement is shown in

Table 1 Reference state

Quantity	Symbol	Value	Ref.
Temperature	T	873 K	
Enthalpy and entropy of oxygen vacancy formation	ΔH and ΔS	Function of x	[19]
Anode gas		50% H_2O +50% H_2→$pO_2=10^{-23.9}$ atm at 873 K	
Cathode gas		Air→pO_2=0.209 atm at 873 K	
Electrolyte thickness	L	10 μm	
External resistance	r_{ext}	Varied parameter	
Anode polarization resistance	r_{anode} (Ni-YSZ)	$1.3 \cdot 10^{-9}\Omega m^2 \cdot \exp\left(\frac{77\frac{kJ}{mol}}{RT}\right) \rightarrow (5.33 \cdot 10^{-5}\Omega m^2 \text{ at } 873\text{ K})$	[20, 21]
Cathode polarization resistance	r_{cathode} (LSCF-CG10)	$2.5 \cdot 10^{-12}\ \Omega m^2 \cdot \exp\left(\frac{116\frac{kJ}{mol}}{RT}\right) \rightarrow (2.15 \cdot 10^{-5}\Omega m^2 \text{ at } 873\text{ K})$	[3]
Ionic charge carrier mobility	μ_i	$\mu_i T$=0.02925exp(−65.18 kJ/RT) m^2/Vs	[18]
Electronic charge carrier mobility	μ_e	$\mu_e T$=0.8433exp(−76.81 kJ/RT) m^2/Vs	[18]

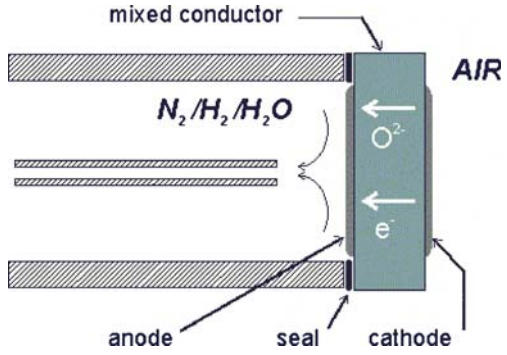

Fig. 2 Measurement setup of the permeation flux measurement

Fig. 2. The sample was exposed to dry flowing mixtures of N_2/H_2 on the inner compartment and air on the outer. The water vapor concentration in the N_2/H_2 exhaust was monitored using a dew point meter (type *Dewlux*, MCM, England) and from this and the known gas flow rate (20N ml/min), the internal short circuit currents in the CGO were calculated via Faraday's law. The currents were converted to current densities using the geometric area of the cell, namely 0.28 cm^2. Measurements were performed at 823 K, 873 K, and 923 K.

Model validation

CG10 conductivity

The model relies on data of the enthalpy and entropy of formation of oxide vacancies and electron and ion mobility data (see the Reference cell section). To evaluate these data, comparisons of the measured and model-derived data of the total conductivity of bulk CG10 were made.

There is good agreement between the total conductivity plots of the model and the experimental data reported by

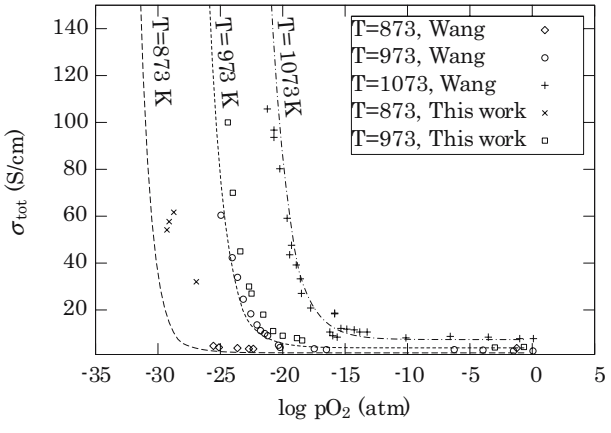

Fig. 3 Total conductivity of CG10 plotted as a function of pO_2. The figure contains data reported by Wang et al. [19] and measurements (*points*) and model calculations (*lines*) from this work

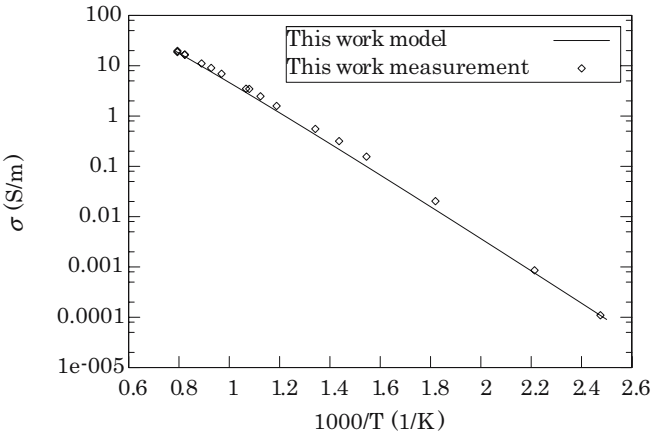

Fig. 4 Total conductivity in air as function of temperature. Measured data of this work (*points*) are compared with calculated data of the model (*line*). To calculate the total conductivity, the model uses data reported by Wang et al. [18, 19]

Wang et al. [19] shown in Fig. 3. This is not surprising because both the mobility data and the thermodynamic data used in the model are those reported by Wang et al.

The measurements of this work are in fair agreement with those of Wang et al. [19] at 873 K. Any discrepancy can be attributed to differences in measurement conditions of the measurements in this work and those of Wang et al. At 973 K, Wang et al. have only a few measurements under strongly reducing conditions. A small deviation between model and the experimental results of this work is observed. The measurements indicate that the pO_2 range in which the electronic conductivity exceeds the ionic conductivity is underestimated in the modeling. It should therefore be noted that the model values might underestimate the leak current.

An Arrhenius plot of the total conductivity data measured in this work and the model calculated total conductivity data is displayed in Fig. 4. There is good agreement between the measured and model-derived data. This suggests that the data reported by Wang et al. used for calculating the vacancy concentration and conductivities in the model describe the total conductivity in the high pO_2 regime well.

Leak current through a CG10 disk

Leak current density data obtained by oxygen permeation measurements on a 210-μm CG10 disk are compared with the model data in Fig. 5. The discrepancy between measured and model derived values is 14% to 40% of the measured values. This is a fair agreement given the precision of the model input data, the intrinsic deviations of real systems from model behavior, and the precision of the measured data.

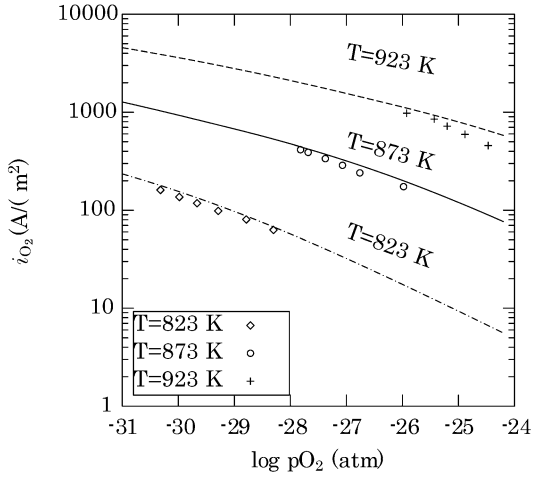

Fig. 5 Leak current density in a 210-μm thick CG10 electrolyte as a function of pO_2 and temperature. Measurements of this work (*points*) is compared to model calculations (*lines*). To calculate the total conductivity, the model uses data reported by Wang et al. [18, 19] for the electrolyte and data reported by Wei Wang et al. [3] for the cathode. The anode is based on values of Primdahl et al. [20] and Barfod et al. [21]

Cell characteristics

Leah et al. [16] have experimentally characterized the electrical performance of a CG10-based fuel cell at 873 K. The CG10 electrolyte was 15-μm-thick. The fuel gas was 97% H_2 + 3% H_2O and the cathode gas was air. The data of Leah et al. are shown in Fig. 6 with two curves calculated from the model outlined in Theory and model description

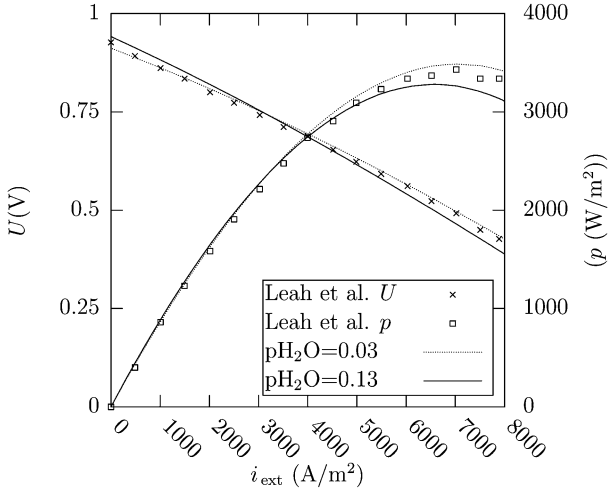

Fig. 6 Cell voltage and power density of a loaded fuel cell. The *discrete points* are measurements reported by Leah et al. [16] on a CG10-based fuel cell with 15-μm-thick CG10 electrolyte at 873 K. The anode gas used by Leah et al. was 97% H_2 + 3% H_2O. The *lines* are model-calculated values of an equivalent cell. The model cell uses $r_{cathode}$=5.5×10^{-5} Ωm^2 and r_{anode}=2.0×10^{-5} Ωm^2. The electrolyte is modeled using the data of Wang et al. [18, 19]. The *two lines* represent model results for an anode gas with 97% H_2 + 3% H_2O and 87% H_2 + 13% H_2O

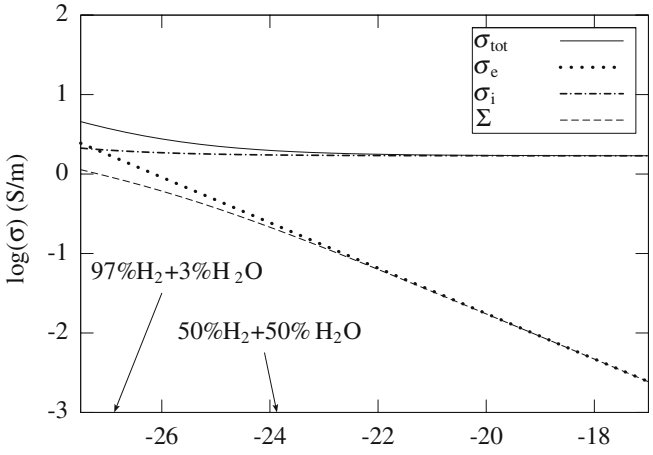

Fig. 7 Conductivities as a function of surrounding atmosphere. T=873 K. Σ, as defined in Eq. 6, is plotted for OCV, i.e., σ_{ext}=0

section. One set is with a 97% H_2 + 3% H_2O gas mixture, which should be valid at low currents. The other is with a gas mixture with 87% H_2 + 13% H_2O, which should be valid at about 8,000 A/m^2 considering the gas flows used by Leah et al. [16]. To achieve agreement between the model curves and the data of Leah et al., the anode polarization resistance used in the model was changed from the reference case value of 5.33×10^{-5} Ωm^2 to 2.0×10^{-5} Ωm^2. The cathode polarization resistance was changed from the reference case value of 2.15×10^{-5} Ωm^2 to 5.5×10^{-5} Ωm^2. Adjusting the electrode polarization resistances in this manner makes the model and the measured data agree.

The agreement in performance of the model cell and of the real cells suggests that the model is capable of simulating the characteristic features of a cell based on a CG10 MIEC electrolyte. The agreement also shows that the reference case values used in this study are close (within a factor of 3 for the electrodes) to a set of values, which will reproduce the cell characteristics as reported by Leah et al.

Modeling results

Ionic and electronic conductivity

The model-calculated pO_2-dependence of the ionic and electronic conductivity at T=873 K is shown in Fig. 7. In the high pO_2 regime, the ionic conductivity is almost independent of pO_2 because the contribution to the oxide charge carrier concentration from the redox reaction (Eq. 2) is small. For the same reason, the electronic conductivity is very small compared to the ionic conductivity at pO_2, which is higher than 10^{-23} atm. Therefore, the electronic conductivity determines Σ. At a pO_2 of about 10$^{-27.5}$ atm, the electronic and ionic conductivities are equal in magnitude and at a pO_2 lower than 10^{-29} atm, the ionic conductivity is much smaller than the electronic conductivity. In this regime, Σ is therefore determined by the ionic conductivity. The increase in ionic conductivity below 10^{-28} atm is not realistic because the associated increase in ionic charge carriers will inhibit the

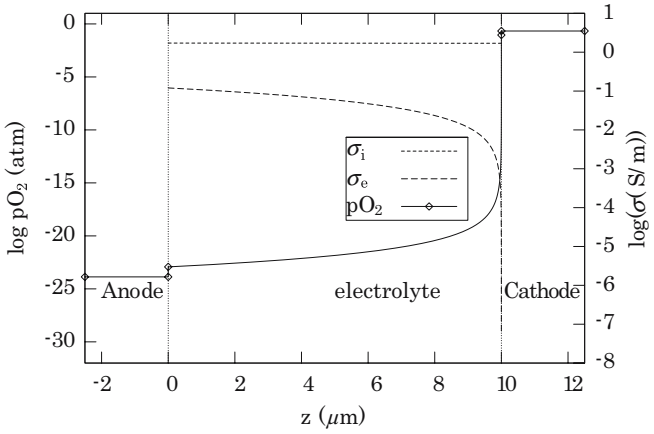

Fig. 8 Conductivities and pO_2 profile of a cell. T=873 K. Open circuit conditions. The anode gas is 50% H_2O + 50% H_2. Thickness is 10 μm

ionic mobility. Therefore, this study is limited to the regime where the ionic conductivity is constant.

pO_2 profile through the cell under open circuit and loaded conditions

The pO_2 profile and the ionic and electronic conductivity profiles across a cell in open circuit conditions are plotted in Fig. 8. The voltage between the electrodes is 0.942 V, which is smaller than the Nernst voltage of 1.004 V. This voltage reduction is due to the electrode polarization and the ohmic loss in the electrolyte caused by the leak current. The ionic conductivity is nearly constant throughout the electrolyte, while the electronic conductivity becomes very small close to the cathode. The pO_2 experiences a small jump at each interface due to the electrode polarization.

The pO_2 and the ionic and electronic conductivity is plotted in Fig. 9 as a function of position in the cell with an applied external load resistance of 8×10^{-5} Ωm^2. This is the load resistance, which provides the largest power p possible under these operating conditions. The voltage between the electrodes is 0.56 V. When loaded, the increased Σ increases the ionic current density. The larger ionic current density increases the electrode polarization. This has the effect of fixing the electrolyte at a pO_2 between 10^{-16} atm and 10^{-5} atm. In this regime, the electronic conductivity is very low compared to the ionic conductivity. In effect, the CG10 electrolyte has become a much better electrolyte than at OCV. This shielding of the electrolyte from the reducing conditions of the anode gas will be referred to as the anode-shielding effect.

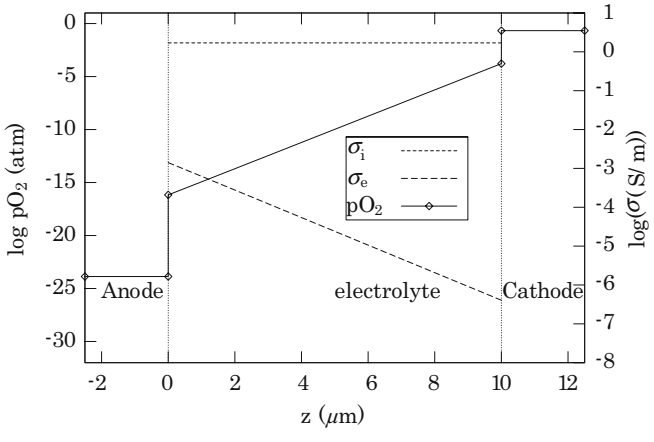

Fig. 9 Conductivities and pO_2 as a function of position. T=873 K. An external load resistance of $r_{ext}=8\times10^{-5}$ Ωm^2 was connected. The anode gas is 50% H_2O + 50% H_2. Thickness is 10 μm

The coupling of leak current density and efficiency

The electronic leak current density i_e is strongly dependent on the operation voltage of the cell. This is illustrated in Fig. 10a where the leak current density at different temperatures are plotted as a function of the cell voltage. Loading of the cell is effectuated by reducing the external resistance, resulting in an increase of i_{ext} and a decrease of U. It is interesting that it is not only the fraction of electrons that runs through the electrolyte that gets reduced when current is allowed to run in the external resistor. It is also the absolute electronic leak current density that is reduced. As temperature is decreased, only a moderate decrease of voltage is required to reduce the electronic leak current density to insignificant levels.

The efficiency $\eta = \frac{U}{U_{Nernst}} \frac{i_{ext}}{i_i}$ and its two factors are plotted in Fig. 10b as functions of i_{ext}. CG10-a denotes a CG10 MIEC while CG10-b denotes a perfect CG10 electrolyte (i.e., the electron mobility was set to nil). Under open circuit conditions, the entire electronic current runs as a leak current through the electrolyte (the situation shown in Fig. 8). This gives a faradaic efficiency of nil. At high current densities, the electronic current runs in the external circuit (the situation shown in Fig. 9). This gives a faradaic efficiency very close to 1. The deviation from U_{Nernst} of U can be divided into two terms according to Eq. 11. The term proportional to i_{ext} is the load term and the term proportional to i_e is the leak term. The leak term is the difference between the voltage of CG10-a and CG10-b. The load term is the difference between the Nernst voltage and the voltage of CG10-b and is a consequence of the external current. For the reference set of parameters (T=873 K), current densities below 500 A/m^2 makes the leak term the largest term. At current densities exceeding 500 A/m^2, the load term is the largest term.

The efficiency of a CG10 cell is at very low current densities determined by the leak current density dominance of the electronic current density (i.e., $\frac{i_{ext}}{i_i}$ is very low) and to some degree, the leak current density term of the voltage efficiency. At high current densities, the CG10 layer shows electrolytic behavior and the efficiency is determined exclusively by the load term of the voltage deviation. This load term is also found in perfect electrolytes. CG10 thus performs as a perfect electrolyte at high current densities.

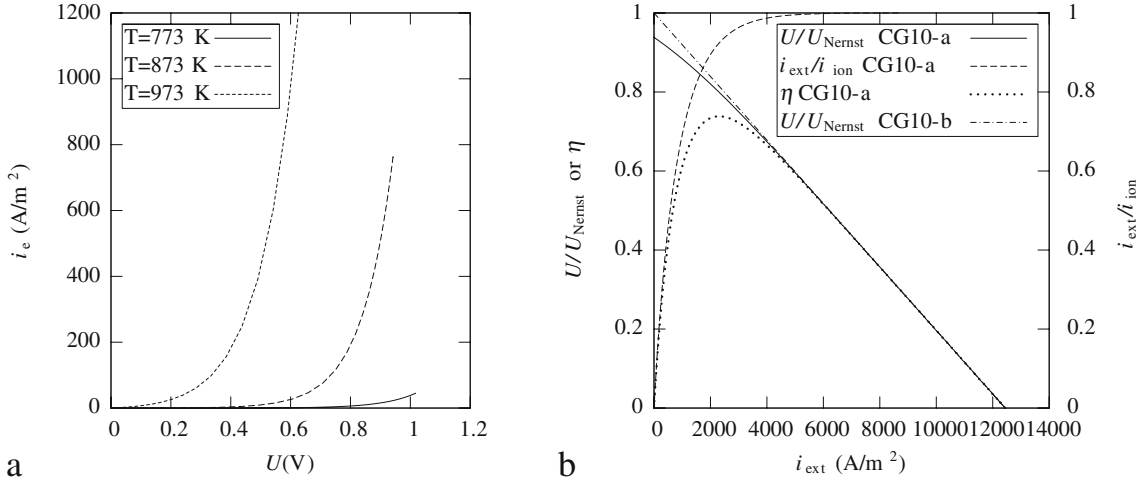

Fig. 10 **a** Electronic leak current density as a function of temperature and cell voltage. T=873 K. L=10 μm. The anode gas is 50% H_2O + 50% H_2. **b** Faradaic efficiency, voltage efficiency, and η of a reference cell (CG10-a) plotted as functions of i_{ext}. For comparison, the voltage efficiency of a perfect CG10 electrolyte (CG10-b) is also plotted. T=873 K. L=10 μm. The anode gas is 50% H_2O + 50% H_2

Temperature-dependence of performance

The mobilities of the ions and the electrons, the cathode and anode polarization resistances, and the charge carrier concentrations are all thermally activated and all affect the oxide stoichiometry and transport parameters of a CG10-based cell. The ionic flux through a loaded cell will be enhanced with increasing temperature due to these activated processes. The temperature-dependence of the efficiency of the cell will, however, depend on whether the ionic or the electronic current density gets the largest enhancement from the increase in temperature.

The efficiency is plotted as a function of the power density at different operation temperatures in Fig. 11a. The highest power density is found at the high temperature due to the increase in ionic conductivity and decrease in polarization resistance, while the highest efficiency is found at low temperature due to the lower concentration and mobility of electronic charge carriers.

In Fig. 11b, the η_{max} and the power density at η_{max} is plotted for different temperatures. Increasing the temperature will cause an almost linear decrease in efficiency. The activation enthalpy of electronic charge carrier formation (Eq. 2) is around 450 kJ/mol and the activation energy of the electron mobility is about 75 kJ/mol, giving a total activation energy in excess of 500 kJ/mol. This is much larger than the activation energies of both the electrode polarization resistances and the ionic conductivity (which are all less than 120 kJ/mol). Therefore, r_e has the strongest temperature-dependence of the resistances in Eq. 12. As r_e decreases when the temperature increases, the efficiency will also decrease (see Eq. 12). Because the ionic mobility and the electrode polarization resistances are thermally activated processes, the power increases with temperature.

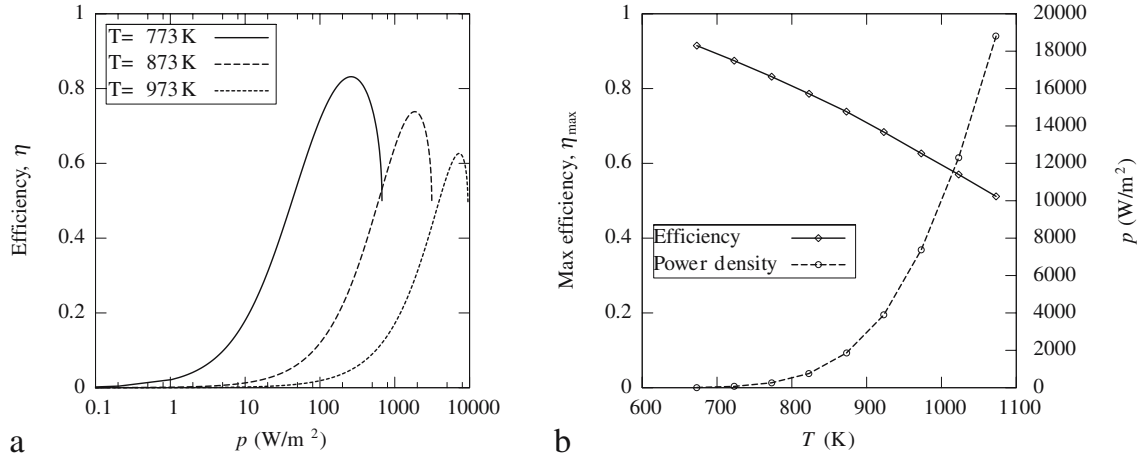

Fig. 11 **a** Efficiency as a function of power density and temperature. L=10 μm. The anode gas is 50% H_2O + 50% H_2. **b** Power density at as function of temperature. L=10 μm. The anode gas is 50% H_2O + 50% H_2

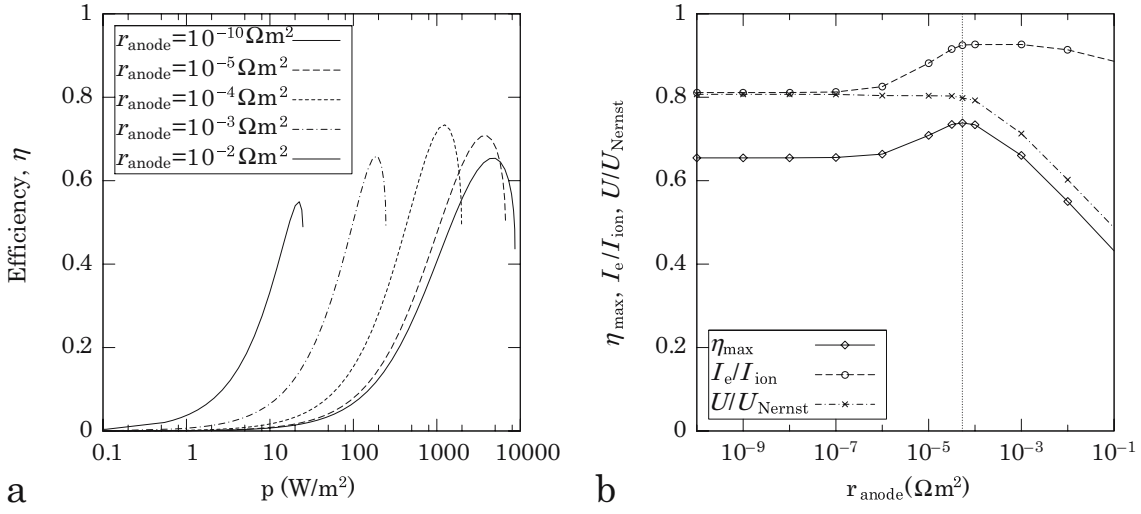

Fig. 12 **a** Efficiency as a function of power density and anode polarization resistance. T=873 K. L=10 μm. The anode gas is 50% H_2O + 50% H_2. **b** Maximum efficiency, η_{max}, faradaic efficiency i_{ext}/i_i at η_{max}, and voltage efficiency at U/U_{Nernst} at η_{max}. T=873 K. L=10 μm. The anode gas is 50% H_2O + 50% H_2. The *vertical line* marks the reference cell anode polarization resistance

At sufficiently high temperatures, however, the reduction of the voltage efficiency will reduce the power of the cell as the cell short circuits internally. This is in contrast to what is observed in cells with perfect electrolytes.

Effects of anode polarization

In Fig. 9 it was shown that when a load was applied, the anode polarization shielded the electrolyte from the reducing anode gas. The electrolyte was therefore not reduced as much as it would have been under open circuit conditions and due to the resulting very low electronic carrier density, the CG10 electrolyte was transformed into a true electrolyte. An anode polarization resistance of sufficient magnitude is required to effectively shield the electrolyte. Increasing the anode polarization resistance, however, will limit the oxide current density.

Figure 12a shows the efficiency as a function of the power density for a range of anode polarization resistances. For large anode polarization resistances, the power density is reduced by the polarization loss at the anode. At small anode polarization resistances, the power density reaches its maximum but the efficiency suffers because the electronic conductivity of the electrolyte is high due to a weak anode-shielding effect.

In Fig. 12b, the η_{max}, the faradaic efficiency at η_{max}, and the voltage efficiency at η_{max} are plotted as functions of the anode polarization resistance. The anode resistance of the reference case (marked by the vertical dotted line) in Fig. 12b is quite close to the resistance where the maximum η_{max} (75%) is achieved. A further reduction of the

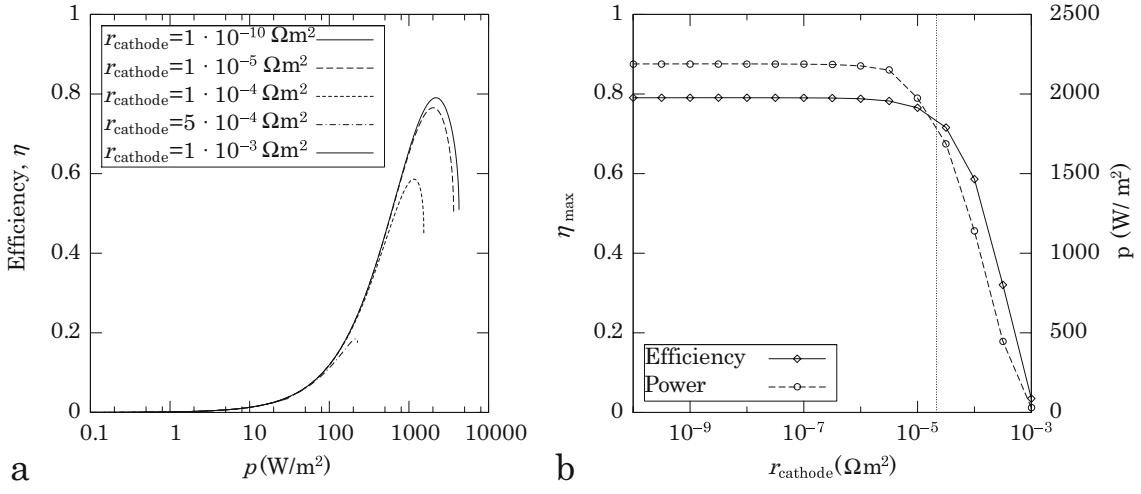

Fig. 13 **a** Efficiency as a function of power density and cathode polarization resistance. T=873 K. L=10 μm. The anode gas is 50% H_2O + 50% H_2. **b** η_{max} and power density at maximum efficiency as function of the cathode resistance. The *vertical line* marks the reference cell cathode polarization resistance. T=873 K. L=10 μm. The anode gas is 50% H_2O + 50% H_2

polarization resistance results in poorer η_{max} (66%). This is a noteworthy result because it means that the anode resistance can in fact become too low. This is even more important when using a fuel gas of lower pO_2 or when increasing the temperature of the cell relative to the reference conditions.

To explain the shape of the curves in Fig. 12b, one must realize that the polarization resistance does not necessarily affect the *maximum* efficiency, η_{max}, of a cell (even though it will reduce the efficiency at some loads). A cell with a perfect electrolyte will be able to reach an efficiency of 1 (see Eq. 12) regardless of polarization resistance in the limit of $i_{ext} \rightarrow 0$.

Equation 12 shows the dependence of the efficiency on the different resistances of the cell. When one keeps in mind the dependence of r_e on r_{anode} through the anode-shielding effect, the anode resistance-dependence of the efficiency can be analyzed.

When the anode polarization resistance is less than 1×10^{-7} Ωm^2, the system is insensitive to changes of r_{anode} as it is too small to influence the voltage efficiency or to inflict any anode-shielding effect.

When 1×10^{-7} $\Omega m^2 < r_{anode} < 5\times10^{-5}$ Ωm^2, the anode-shielding effect increases r_e significantly. This leads to an increase in the faradaic efficiency. In this regime, r_{anode} is of the same order of magnitude or less than $r_{cathode}+r_{ion}$. The detrimental effect on the voltage efficiency of an increase in r_{anode} is thus diluted by $r_{cathode}+r_{ion}$. Therefore, the benefits of the shielding effect on both the faradaic and the voltage efficiency will give a net increase in efficiency when r_{anode} is increased within this range.

When $r_{anode} > 5\times10^{-5}$ Ωm^2, r_{anode} will severely limit the ion current density. The anode-shielding effect will thus benefit less in this regime from an increase of r_{anode} as the anode polarization is the product of r_{anode} and i_i. Furthermore, r_{anode} is now larger than $r_{cathode}+r_{ion}$ and the voltage efficiency is thus very sensitive to r_{anode}. The net effect is that the voltage efficiency is reduced when r_{anode} is increased.

When r_{anode} becomes very large, r_{ext} will have to be of the same order as r_{anode} to keep up the voltage efficiency. At the same time, it is not beneficial for r_{ext} to be much larger than r_e as the faradaic efficiency will decrease. It turns out that to get η_{max} when increasing r_{anode}, it is necessary to increase r_{ext} a bit faster than r_e is increased and as a result, i_{ext}/i_i will be decreased for very large values of r_{anode}.

Effects of cathode polarization

The efficiency and the power density of a cell calculated for different cathode polarization resistances are shown in Fig. 13a. Contrary to a high r_{anode}, a high $r_{cathode}$ will shield the electrolyte from high pO_2. This will reduce the electrolyte and decrease r_e. This is the cathode-shielding effect. Contrary to the anode-shielding effect, the cathode-shielding effect is detrimental to the electrolyte performance. The impact of the cathode-shielding effect is however, smaller than the anode-shielding effect because the high pO_2 parts of the electrolyte has lower electronic conductivity than the low pO_2 parts and thus contribute less to the integral in Eq. 5. Equation 12 states that the combination of a large $r_{cathode}$ and a small r_e decreases both the faradaic and the voltage efficiency as can be seen in Fig. 13b. At $r_{cathode} < 10^{-7}$ Ωm^2, the detrimental effect of the cathode polarization resistance becomes insignificant. A decrease of the cathode polarization resistance from the reference state (vertical dotted line) will, however, increase both power density and efficiency.

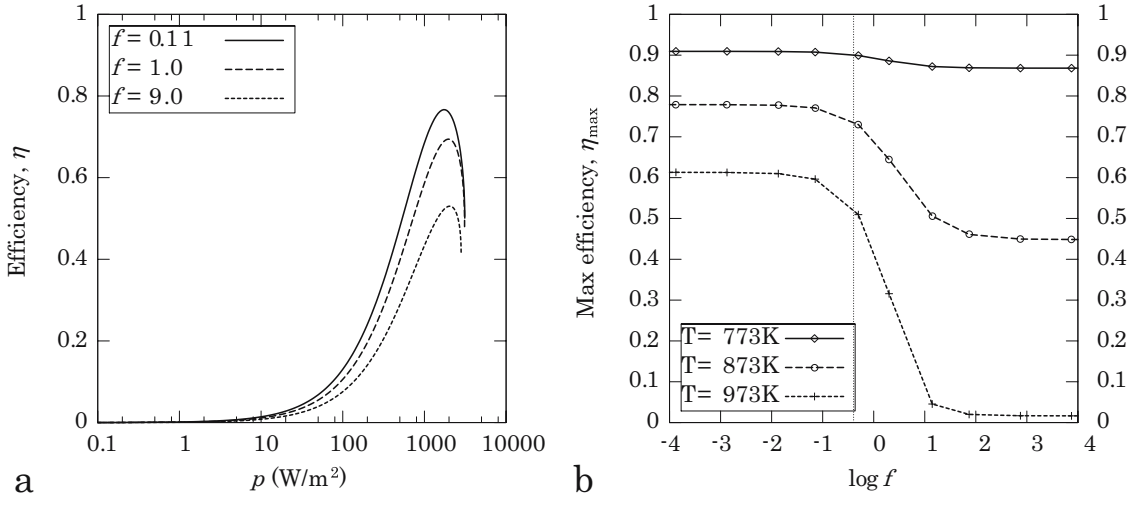

Fig. 14 **a** Efficiency as a function of power density and values of $f = r_{cathode}r_{anode}$. $r_{anode}+r_{cathode}=7.5\times10^{-5}$ Ωm^2. T=873 K. L=10 μm. The anode gas is 50% H_2O + 50% H_2. **b** η_{max} as function of $f = r_{cathode}r_{anode}$ and temperature. The *vertical dotted line* marks the reference cell. T=873 K. $r_{anode}+r_{cathode}=7.5\times10^{-5}$ Ωm^2. L=10 μm. The anode gas is 50% H_2O + 50% H_2

Effects of the electrode polarization distribution

When a large ionic current density is flowing through a CG10-based cell for a given set of parameter values, Fig. 9 shows that a significant pO_2 gradient is found on the electrodes. In the previous paragraphs, it was shown that the cathode and the anode polarization resistances influence the performance of the cell partly by their polarization loss, and partly by the anode- and cathode-shielding effects.

The efficiency as a function of the power density is plotted in Fig. 14a for a range of cathode to anode polarization resistance ratios *f*. The total electrode polarization resistance ($r_{cathode}+r_{anode}$) was kept constant and the ratio of cathode to anode polarization resistance (*f*) was varied.

Figure 14b, which shows the maximum efficiency at different temperatures and values of *f*, states that at large values of *f* a low efficiency and power density is achieved while at small values of *f* a high efficiency and power density is achieved. As the total electrode polarization resistance is constant, this is entirely an effect of the pO_2 in which the electrolyte is operating, which is determined by the distribution of the electrode polarization between the cathode and the anode. Furthermore, as the sensitivity of r_e to the pO_2 is dependent on the operating temperature, the anode and cathode shielding becomes much more critical at high temperatures. At 773 K, the efficiency could be changed from 87% to 91% while keeping the total polarization resistance constant. At 973 K, the efficiency could be changed from 18% to 62% while keeping the total polarization resistance constant. The temperature-dependence reflects the larger significance of the shielding effects due to easier reduction of the electrolyte at high temperatures.

Thickness-dependence

One way to increase the ionic current densities through a cell is to reduce the thickness of the electrolyte. This reduces the electrolyte resistance of ions but increases the electronic conductivity.

The efficiency is plotted as a function of the power density for three different values of electrolyte thickness in Fig. 15a. Making electrolytes thinner than 10 μm will yield a small increase of power density at the expense of a considerable reduction of η_{max}.

In Fig. 15b, η_{max}, the faradaic efficiency, and the voltage efficiency is plotted as a function of the electrolyte thickness *L*. A reduction of the electrolyte thickness will reduce the ionic resistance of the electrolyte. At thicknesses larger than 10^{-5} m, any thickness reduction will therefore lead to an increased ionic current density and therefore larger electrode polarizations. This will in turn increase the anode- and cathode-shielding effects and decrease σ_e. As r_e is proportional to both *L* and σ_e^{-1}, the anode-shielding effect will ensure that r_e will actually increase a bit as *L* is decreased. When *L* becomes less than 10^{-5} m, the increase in current density levels off because most of the cell resistance is located at the electrodes. Therefore, below this thickness, σ_e will be constant as the anode polarization has reached its maximum and when *L* is decreased further, r_e will decrease. As Eq. 12 states, this will have a detrimental effect on both the voltage and the faradaic efficiency.

It seems that little effort should be put into creating electrolytes thinner than 10 μm because this has a detrimental effect on performance.

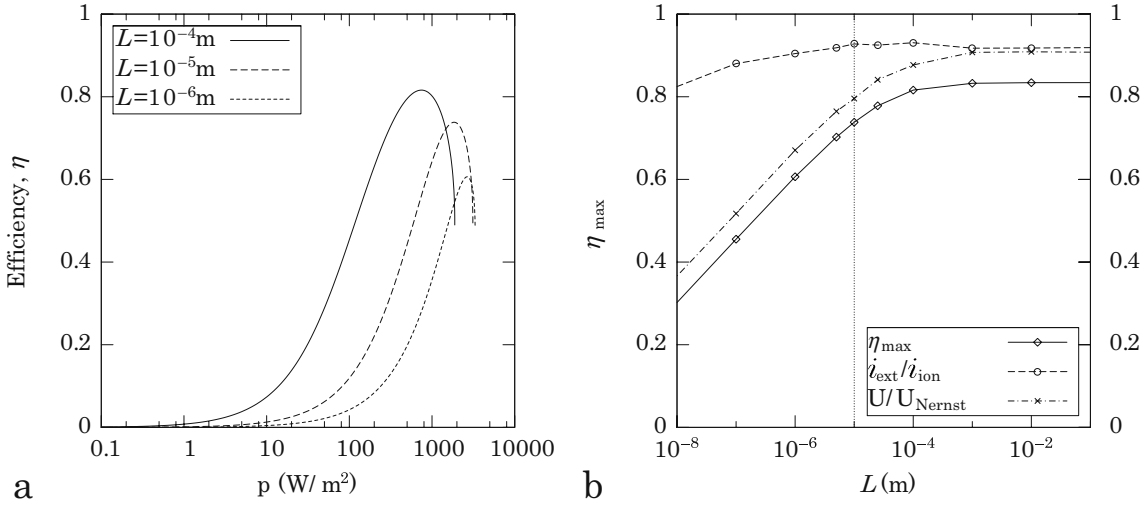

Fig. 15 **a** Efficiency as a function of power density and electrolyte thickness, *L*. *T*=873 K. The anode gas is 50% H_2O + 50% H_2. **b** Plot of the η_{max}, the faradaic efficiency at η_{max}, and the voltage efficiency at η_{max} as function of the thickness *L* of the CG10 electrolyte. *T*=873 K. The anode gas is 50% H_2O + 50% H_2

Nanocrystalline CG10 electrolytes and the importance of the vacancy-formation enthalpy

Suzuki et al. [23] investigated the effects of grain size on the defect chemistry of doped and undoped ceria. They found that fine-grained samples of CG20, CG10, and pure ceria has a significantly lower vacancy-formation enthalpy than coarse-grained samples. The low enthalpy of the fine-grained samples is caused by their larger concentration of grain boundaries, which are believed to be easily reduced. The lower vacancy-formation enthalpy of fine-grained samples creates comparably more electronic charge carriers for a given pO_2 and temperature. For each gadolinia concentration, Suzuki et al. found a threshold diameter (less than 20 nm). This threshold diameter decreases as the gadolinia content increases. Chiang et al. [24, 25] found that the enthalpy of oxide vacancy formation in pure ceria with grains 10 nm in diameter was half that of the bulk, resulting in an electronic conductivity 10^4 times larger than that of bulk ceria. In the heavily doped composition of $Ce_{0.74}Gd_{0.26}O_{1.87-x}$ (CG26), Chiang et al. found no increase in electronic conductivity with grain diameters as low as 10 nm compared to coarse-grained samples, in accordance with the findings of Suzuki et al. Recently, however, J. Rupp (personal communication) has reported enhanced electronic conductivities to be found in thin CG20 films with grain sizes up to 60 nm. This suggests that the threshold diameter depends on other factors despite the gadolinia content. Furthermore, while a very high gadolinia content will prevent the reduction of the grain boundary, a high dopant content will dramatically decrease the ionic conductivity due to trapping of the ionic charge carriers [1].

Calculated IV curves of a cell based on a 10-μm-thick CG10 electrolyte using different oxide vacancy-formation enthalpies are plotted in Fig. 16a. An enthalpy reduction of 5% of the reference value H_0 results in a reduction of 10% of the OCV. At higher fluxes, the difference of the reference case and the cases with reduced oxide vacancy-formation enthalpy is reduced. A 10% increase in enthalpy gives an OCV close to the Nernst voltage (marked by a circle on the U axis).

In Fig. 16b, η is plotted as a function of the power density produced using different oxide vacancy-formation enthalpies. Both the efficiency and the power density are dependent on the enthalpy of oxide vacancy formation. The lowering of the ionic charge carrier concentration created by increasing ΔH has no detrimental effect on the maximum achievable power reflecting that the vast majority of vacancies are created by gadolinia substitution of ceria. A 10% increase in the oxide vacancy-formation enthalpy will give a maximum efficiency of about 8% larger than a normal CG10 cell. A CG10 fuel cell with a ΔH lower than the reference value will however be unlikely to achieve a high maximum efficiency. Fine-grained CG10 electrolytes with correspondingly low vacancy-formation enthalpy could find applications as oxygen separation membranes though, especially at elevated temperatures, due to their high σ_i.

Comparison with state-of-the-art zirconia-based electrolytes

If CG10 should be successful as an electrolyte in a fuel cell, it must compare well with other candidate electrolytes. For comparison, the electrolyte $Zr_{0.79}Ce_{0.01}Sc_{0.20}O_{1.9}$ (ZrScCe) with ionic conductivities reported in Mogensen et al. [10] will be used. The electronic conduction in ZrScCe is assumed to be nil. The anode polarization resistance will be assumed to be equivalent to that of the CG10 cells. State-of-the-art zirconia-based cells have inferior cathodes compared with their ceria-based counter-

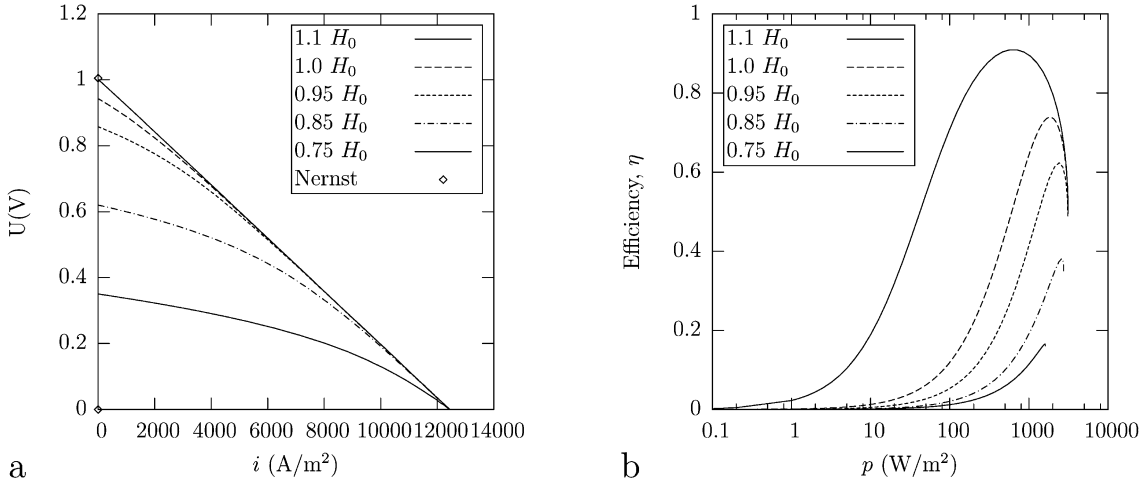

Fig. 16 **a** IV plot of a CG10-based cell. Plots are for CG10 and CG10 with modified vacancy formation enthalpies. The *labels* state the enthalpies as a function of the bulk enthalpy H_0. T=873 K. L=10 μm. The anode gas is 50% H_2O + 50% H_2. **b** Efficiency as a function of power density and vacancy formation enthalpy. Plots are for CG10 and CG10 with modified vacancy formation enthalpies. The labels state the enthalpies as a function of the bulk enthalpy H_0. T=873 K. L=10 μm. The anode gas is 50% H_2O + 50% H_2

parts. Wang et al. [27] has reported the performance of a $(La_{0.75}Sr_{0.25})_{0.95}$ MnO_3 (LSM) cathode for zirconia-based cells with the following temperature-dependent polarization resistance:

$$r_{\text{cathode}} = 1.40 \times 10^{-11}\,\Omega\text{m}^2 \cdot \exp\left(\frac{122\,\frac{\text{kJ}}{\text{mol}}}{RT}\right) \quad (13)$$

At 873 K, this cathode polarization resistance is roughly eight times larger than the one used for the CG10 cell.

The efficiency as function of the power density is shown in Fig. 17a for different cells. Comparing ZrScCe-a (ZrScCe with its usual cathode resistance) and ZrScCe-b (ZrScCe with the CG10 cathode resistance), it is clear that the cells are very sensitive to the cathode resistance as decreasing the cathode resistance eightfold increases the power density fivefold at 873 K.

ZrScCe-b and CG10-b (CG10 where the electronic conduction is set to nil) are nearly identical because their ionic conductance are similar.

Comparing CG10-a (normal CG10) and CG10-b, they are identical at the point of maximum power density output. At lower power, they diverge as the leak current density begins to build in CG10-a, which reaches an $\eta_{\max}$ value of 0.74.

Comparing CG10-a with ZrScCe-b, these points still stand. If cathodes comparable to the ones available for CG10 are developed for ZrScCe cells, the ZrScCe cell will surpass the performance of the CG10 cells at temperatures higher than 873 K. Simulations at 773 K (not shown) shows that at lower temperatures CG10 will have an advantage at high-power density due to a larger ionic conductivity at low temperatures, even when similar electrodes are used.

At a given efficiency, CG10-a can provide about four times the power density that ZrScCe-a can provide. When approaching open circuit conditions, CG10 reaches its $\eta_{\max}$ of 0.74 and if higher efficiencies are required, CG10 is not an option.

The power density of a CG10 cell is substantially higher than that of a zirconia cell even when operating at the maximum efficiency of the CG10 cell. Therefore, the important parameter when deciding between a CG10 and a zirconia cell is what efficiency is required of the cell and at what temperature the cell is required to operate. The $\eta_{\max}$ obtainable with a CG10 electrolyte as function of temperature is plotted in Fig. 17b. If the efficiency requirements of a cell are in the bottom left part of the plot, CG10 should be chosen for the electrolyte as it supports higher power densities. If the efficiency requirements are in the top right part of the plot, ZrScCe should be chosen because CG10 is not able to reach adequate efficiency.

One of the arguments for selecting a CG10 electrolyte over a zirconia-based electrolyte is that the leak current density will be small when the cell is strongly polarized and has a large ionic current density. This is the region where the performance curves of CG10-a and CG10-b converge in Fig. 17a. That argument is not good because the efficiency at this point was driven down to about 0.6 by polarization losses. At the point of $\eta_{\max}$, the leak current density is actually about 8% of the ionic current density.

Discussion

Possibilities of improving cells based on CG10 electrolytes

The amount of resources which should be dedicated to enhancing the performance of a specific part of a CG10 fuel cell is related to the relative importance of this part for the performance of the whole cell. Estimating the important

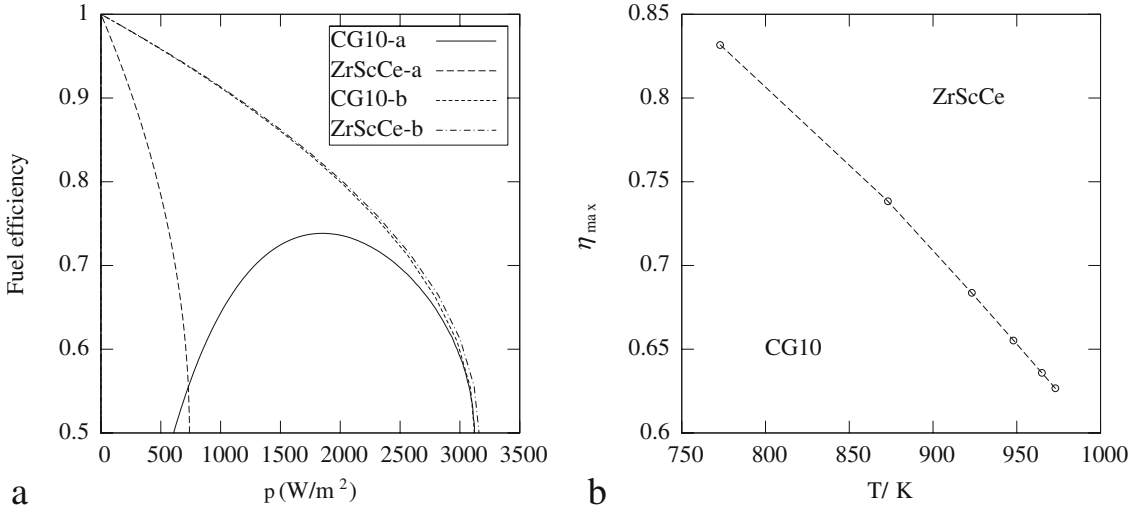

Fig. 17 **a** Efficiency as a function of power density. CG10-a is CG10. ZrScCe-a is ZrScCe with its usual cathode. ZrScCe-b is ZrScCe with a cathode comparable with the CG10 cell electrodes. CG10-b is CG10 with the electronic conduction set to nil. T=873 K. L=10 μm. The anode gas is 50% H_2O + 50% H_2. **b** Plot of the $\eta_{\max}$ of the CG10 electrolyte. L=10 μm. The anode gas is 50% H_2O + 50% H_2

parts is not trivial due to the many related phenomena taking place. What limits the performance under one set of conditions might be irrelevant in another set of conditions. Even the term "performance" is not uniquely defined. Due to the load term of the voltage efficiency, the operation conditions even of fuel cells with a perfect electrolyte will always be a tradeoff between power density and efficiency.

Case 1: high-power density applications

The cost of running a fuel cell power plant contains contributions from both the capital cost of the power plant and the cost of fuel. In the case where the capital and associated depreciation costs are large compared to the fuel costs, a high power density will be preferable to a high efficiency. A high power density will also be advantageous when size-limited systems demand a certain power density for use in, for instance, vehicles or portable devices.

Changing the temperature and the external resistance are ways to quickly increase the power density of a cell. In the longer term, however, the components of the cell could be improved. For the reference cell at 873 K, about 20% more power could be extracted without any loss of efficiency if the cathode polarization resistance was eliminated. Five times more power could be extracted if the anode resistance was eliminated at the cost of reducing the efficiency from 74% to 66%. Reducing the electrolyte thickness will potentially increase the power density by about 20%. Because the power density-limiting parameter is the anode resistance, only a modest benefit of reducing the thickness or cathode resistance is found. If the anode resistance was eliminated, it would again be more feasible to reduce the other parameters. At some point, however, the faradaic efficiency will be so low that the power density will suffer and no further power enhancement could be realized. This is in contrast to cells based on perfect electrolytes, which in the case of an infinitely thin electrolyte with perfect electrodes, as far as the mathematics is concerned, should support an infinitely high power density.

Case 2: high efficiency applications

If the production cost of a fuel cell power plant is sufficiently low compared to the fuel cost, high efficiency becomes vital. This will be the case in larger power plants with long lifetimes. The efficiency η discussed in this study is a *cell efficiency*. In the case of a perfect electrolyte, the upper limit of $\eta_{\max}$ is 1 (Note that this is indeed a limiting case: $\eta_{\max}$ will tend to 1 only in the limit where $i_i \to 0$ where the output power, $p \to 0$). The efficiency of a system built over CG10-based cells will, like for any fuel cell-based system, be lower than dictated by the cell efficiency. The system efficiency may schematically be written: $\eta_{sys} = \eta \cdot FU \cdot \frac{\Delta G}{\Delta H} \cdot \eta_{aux}$ where the second factor *FU* is the fuel utilization reflecting the fraction of the available fuel that is actually converted in the cell, the third factor is the thermodynamic efficiency, reflecting that not all energy in the fuel stream is available for the electrochemical process, and the last term, η_{aux}, represents losses in all other auxiliary components, e.g., blowers and inverters. At 600 K, $\frac{\Delta G}{\Delta H}$ is 82% for a hydrogen-fuelled cell and $\frac{\Delta G}{\Delta H}$ ~1 for a methane-fuelled cell. The achievable fuel utilization and the system losses are strongly dependent on the system. Eighty-five percent is considered a realistic number for the product of η_{aux} and *FU*.

The anode polarization resistance of the reference cell is actually at its optimum when running at 873 K. This optimum could, however move toward lower values of anode resistance if future advances reduced the resistance of other parts of the cell, allowing a higher current density. Eliminating the cathode polarization resistance of the reference cell would increase the maximum efficiency from 74% to 79%.

Increasing the thickness from 10 μm to 100 μm will increase the efficiency from 74% to 82%. The same increase in efficiency would be found by reducing the temperature to 773 K. The power density would be reduced to 40% of the reference case value by increasing the thickness. The power density, however, would be reduced to 14% of the reference case value by reducing the temperature from 873 K to 773 K. Increasing the efficiency by increasing the electrolyte thickness would thus reduce the power density less than a decrease in temperature.

On the other hand, by reducing the operating temperature, the lifetime can be significantly increased if temperature activated aging processes are important. Because the anode-shielding effect will be less important with a low electronic conductivity, it becomes vital to decrease the electrode polarization resistances. This is doubly important because high electrode polarizations can be at least as detrimental to cell performance as high temperatures [28, 29].

A good choice would therefore be to increase the thickness of the cell and reduce the cathode resistance. Further optimizations would be achieved by lowering of the temperature and adjusting the anode polarization resistance.

Finally, as pointed out by Matsui et al. [14], an increase of the pO_2 of the fuel gas will increase the efficiency of doped ceria cells. Doped ceria cells could be placed downstream from zirconia-based cells and only be exposed to fuel with large water content to prevent reduction of the CG10 electrolyte.

Considerations of CG10 or zirconia

Compared to conventional "perfect" electrolytes such as zirconia, the lower cathode polarization resistance is the main advantage of CG10. This allows CG10 to have a significantly higher power density than zirconia electrolyte-based cells. Another advantage is a higher ionic conductivity below 873 K. The disadvantages include a maximum efficiency and a lower limit to the thickness of the electrolyte due to the electronic leak current density.

The reference CG10 electrolyte-based cell is able to support higher power densities than state-of-the-art zirconia-

based cells at low to intermediate temperatures. Furthermore, if the power density is increased beyond the point of η_{max}, the efficiency will actually approach that of zirconia-based cells. In this case, CG10 will be the better choice for the electrolyte. The requirements for power density could also be so high that the temperature has to be increased to support them. A very high temperature will make zirconia-based cells the best choice, in part because the cathode performance matters less at high temperature and, in part because CG10 is easily reduced at high temperature.

The reference CG10 cells have a limit to their maximum efficiency. When the required efficiency exceeds this limit, zirconia-based cells will be required. If, on the other hand, it is possible to optimize the CG10 cells to meet the required efficiency, CG10 should be considered as electrolyte. CG10 has the advantage of a higher power density compared to zirconia cells at equal efficiency especially at T<873 K. Among the drawbacks are a narrow power density range at which the CG10 cell operates close to η_{max}. A cell with a perfect electrolyte will, in periods of low power consumption, be able to reduce fuel consumption by increasing the load resistor and be able to gain efficiency. These good part load characteristics are not shared by CG10-based cells. A CG10 cell will, if the load resistor is increased, reduce its efficiency and will thus not reduce its fuel consumption as much as a perfect electrolyte would. Reducing the temperature would be an alternative way to reduce fuel consumption in a CG10 cell, but although the efficiency will be increased, frequent temperature cycles could possibly have a detrimental effect on the cell lifetime.

The above discussion centers around the reference CG10 cell, which is based on the state-of-the-art technology of late 2005. Future developments could change the situation significantly. If better cathodes for zirconia-based cells were developed, much of the advantage of CG10 cells would disappear. At the moment, the possibility of adding a doped ceria layer on top of the zirconia electrolyte to support better cathodes is being investigated. If these good cathodes can be realized for zirconia-based cells, they will be able to provide nearly the same power densities as CG10 cells even below 873 K while maintaining higher efficiencies. So far, the progress has been limited [30–32].

Conclusions

A model combining established defect chemistry and ambipolar transport theory was applied to a fuel cell based on a CG10 electrolyte. The model is able to reproduce measurements of total conductivity of CG10 and permeation flux of a CG10 cell. It was found that CG10 can become a good electrolyte when loaded such that large ionic current are running through it. The efficiency of a CG10 cell can be enhanced by using a thicker electrolyte layer, lowering the temperature, and having a low cathode polarization resistance. Reducing the enthalpy of oxide vacancy formation should be avoided because it decreases efficiency. Compared to zirconia-based cells, CG10 cells supports higher fluxes at a given efficiency but are limited in their maximum efficiency. This makes CG10-based cells a valid alternative to zirconia-based cells in applications where operation at temperatures below 873 K and high-power density is required.

Acknowledgement This work was, in part, supported by the Danish Energy Agency through the project DK-SOFC b long-term SOFC R and D, contract no. 33031-0006.

References

1. Mogensen M, Sammes NM, Tompsett GA (2000) Solid State Ion 129:63
2. Inaba H, Tagawa H (1996) Solid State Ion 83:63
3. Wang WG, Mogensen M (2005) Solid State Ion 176:457
4. Xu X, Xia C, Xiao G, Peng D, Yi B (2005) Solid State Ion 176:1513
5. Zhonge B, Cheng M, Dong Y, Wu H, She Y (2005) Solid State Ion 176:655
6. Xia C, Chen F, Liu M (2001) Electrochem Solid-State Lett 4: A52
7. Hibino T, Hashimoto A, Asano K, Yano M, Suzuki M, Sano M (2002) Electrochem Solid-State Lett 5:A242
8. Zha S, Moore A, Abernathy H, Liu M (2004) J Electrochem Soc 151:A1128
9. Attryde P, Baker A, Baron S, Blake A, Brandon NP, Corcoran D, Cumming D, Duckett A, El-Koury K, Haigh D, Harrington M, Kidd C, Leah R, Lewis G, Matthews C, Maynard N, McColm T (2005) Proc SOFC IX, 113
10. Mogensen M Lybye D, Kammer K, Bonanos N (2005) Proc SOFC IX, 1068
11. Riess I, Gödickemeier M, Gauckler LJ (1996) Solid State Ion 90:91
12. Steele BCH (2000) Solid State Ion 129:95
13. Näfe H (2001) J Appl Electrochem 31:1235
14. Matsui T, Inaba M, Mineshige A, Ogumi Z (2005) Solid State Ion 176:647
15. Virkar V (2005) J Power Sources 147:8
16. Leah RT, Brandon NP, Aguiar P (2005) J Power Sources 145:336
17. Schottky W, Wagner C (1930) WZ Phys Chem B11:11
18. Wang S, Inaba H, Hiroaki T, Dokiya M, Hashimoto T (1998) Solid State Ion 107:73
19. Wang S, Kobayashi T, Dokiya M, Hashimoto T (2000) J Electrochem Soc 147:3606
20. Primdahl S, Mogensen M (1999) Proc SOFC VI, 530
21. Barfod R, Mogensen M, Klemensø T, Hagen A, Liu YL, Hendriksen PV (2005) Proc SOFC IX, 524
22. Appel CC, Bonanos N, Horsewell A, Linderoth S (2001) J Mater Sci 36:4493
23. Suzuki T, Kosacki I, Anderson HU (2002) J Am Ceram Soc 85:1492
24. Chiang YM, Lavik EB, Kosacki I, Tuller HL, Ying JY (1996) Appl Phys Lett 69:185
25. Chiang YM, Lavik EB, Blom DA (1997) Nanostruct Mater 9:633
26. Kupp J (2006) personal communication
27. Wang WG, Barfod R, Larsen PH, Kammer K, Bentzen J, Hendriksen PV (2003) Proc SOFC VIII, 400
28. Koch S, Hendriksen PV, Mogensen M, Liu YL, Dekker N, Rietveld B, Haart B, Tietz F (2006) Fuel Cells - accepted
29. Hagen A, Barfod R, Hendriksen PV, Liu YL, Ramousse S (2006) J Electrochem Soc - submitted
30. Matsuzaki Y, Yasuda I (2002) Solid State Ion 152–153:463
31. Nguyen TL, Kobayashi K, Honda T, Iimure Y, Kato K, Neghisi A, Nozaki K, Tappero F, Sasaki K, Shirahama H, Ota K, Dokiya M, Kato T (2004) Solid State Ion 174:163
32. Shiono M, Kobayashi K, Nguyen TL, Hosoda K, Kato T, Ota K, Dokiya M (2004) Solid State Ion 170:1